Jurnal Teknologi

Full Paper

INVESTIGATION OF THE INJECTION RATE CHARACTERISTICS OF DIESEL SOLENOID INJECTORS IN SINGLE AND SPLIT INJECTION STRATEGIES

Vo Tan Chau*, Hoang Phi Hung

Faculty of Automotive Engineering Technology, Industrial University of Ho Chi Minh City (IUH), Ho Chi Minh City, Vietnam

Article history
Received
28 July 2025
Received in revised form
21 October 2025
Accepted
22 October 2025
Published Online
27 February 2026

*Corresponding author
votanchau@iuh.edu.vn

Graphical abstract

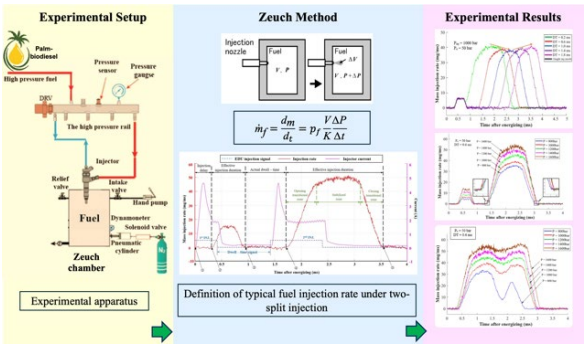

Abstract

Understanding injection rate characteristics, particularly dwell-time variations and split injection behavior under high injection pressure, is essential for optimizing diesel combustion processes. This study experimentally investigates these parameters using the high-precision Zeuch method to measure injection rate profiles and fuel quantities for both single and split injection strategies. Experiments were conducted on a six-hole solenoid injector at rail pressures ranging from 800 bar to 1600 bar. A total energizing duration of 1.4 ms was applied either as a single injection or divided into 30%/70%, 50%/50%, and 70%/30% split ratios, with dwell-times varied from 0.2 to 1.8 ms. Results revealed that the first split injection exhibited a rate profile nearly identical to that of the single injection, regardless of dwell-time variation. In contrast, the second split injection was strongly influenced by fuel pressure oscillations within the injector and rail system. Its average quasi-steady state injection rate decreased from 40.1 mg/ms to 38.5 mg/ms as the dwell-time increased from 0.2 ms to 1.0 ms, and then recovered to 40.0 mg/ms when dwell-time further increased from 1.0 ms to 1.8 ms. Short dwell-times (0.2ms) led to merged injection rate profiles, increasing the injected fuel quantity by approximately 21.1% compared to the 0.6 ms dwell-time case, where the two injections were clearly separated. These findings highlight the critical influence of dwell-time on injection rate characteristics and provide valuable insights for optimizing diesel combustion phasing in split injection strategies.

Keywords: Injection rate characteristics, split injection strategies, Zeuch method, Diesel engine, High-pressure fuel injection

1.0 INTRODUCTION

Diesel engines have been extensively used across various sectors due to their advantages in engine power and high thermal efficiency. However, the emissions generated, particularly nitrogen oxides (NOx) and particulate matter (PM), present serious risks to human health [1, 2, 3]. To reduce these emissions, various technological solutions have been developed to improve parameters influencing the combustion process. Among these, intake air dynamics, in-cylinder chamber geometry, fuel properties, and, in particular, the injection rate play a key role in forming the in-cylinder fuel–air mixture [4, 5, 6, 7]. Precise control of operating parameters in the Common Rail System (CRS) allows modification of the injection rate profile. This approach has become essential for meeting increasingly stringent emissions

regulations. Consequently, optimizing the injection rate is key to enhancing fuel atomization, spray development, and air–fuel mixing quality. Several studies have demonstrated that injection pressure strongly influences both the injection rate profile and emission formation. Benajes *et al*. (2006) and Xu *et al*. (2018) reported that variations in injection pressure significantly influence both the injection rate profile and emission formation [8, 9]. Karra *et al*. (2009) observed that particulate matter (PM) emissions decreased by nearly 60% when the injection pressure increased from 100 to 200 MPa, although NO_x emissions simultaneously rose [10]. Similarly, Han *et al*. (2014) found that higher injection pressure advanced the start of injection and prolonged the effective injection duration, thereby increasing fuel quantity and discharge coefficient [11]. However, elevated injection pressures also generate stronger pressure oscillations in the system, which can affect subsequent injections and cause fluctuations in the injection rate and fuel delivery during split injections. These effects are governed by parameters such as injection timing, injection pulse, injection length distribution ratio, and injection pressure. Manin *et al*. (2012) and Piano *et al*. (2017) confirmed that pressure waves generated in the rail propagate back to the injector, altering the injection rate and injected mass [12, 13]. Similarly, Ferrari *et al*. (2006) pointed out that pressure oscillations caused by pilot injections can increase fuel consumption, particularly under shortened dwell-time conditions [14].

Optimizing the operating parameters of a fuel injection system requires addressing several complex issues, including fuel metering accuracy—such as injection timing, fuel quantity, and injection rate—as well as determining appropriate injection strategies for various engine operating conditions [15]. These adjustments can significantly affect mixture formation and combustion, thereby influencing overall engine performance [16, 17]. Various methods have been developed to characterize high-pressure injection behavior, with the Bosch long-tube and Zeuch methods being the most widely adopted [18, 19]. The Bosch injection rate meter is commonly used as a standard measurement tool, while the Zeuch method provides higher accuracy for determining the shape of the injection rate curve and the start and end of injection. Regarding state-of-the-art injection strategies, pilot injection increases in-cylinder pressure and temperature, leading to earlier ignition, reduced combustion noise, and lower NO_x emissions. The main injection ensures efficient air–fuel mixing for complete combustion, while post-injection reduces PM emissions [20, 21, 22]. Another study by Sindhu *et al*. (2018) reported that a two-split injection strategy with a 25%/75% fuel distribution ratio significantly reduced both PM and NO_x emissions compared to a single injection [23]. Similarly, Nehmer *et al*. (1994) observed that NO_x emissions decreased across different split ratios (25%/75%, 50%/50%, and 75%/25%) [24]. However, extended dwell times were found to lower combustion temperatures and increase PM emissions. Beatrice *et al*. (2002) also reported that as dwell time increased from 490 to 1350 µs, PM emissions rose by approximately 30%, despite the reduction in NO_x [25].

From the aforementioned standpoint, most previous studies have tended to analyze the effects of injection pressure, dwell time, and split ratio individually, without systematically examining their combined and sequential impacts on the injection rate behavior of common-rail diesel injectors. As a consequence, the complex interactions among these parameters have not been sufficiently clarified, leading to a lack of well-defined correlations that are essential for accurately controlling the timing and quantity of high-pressure fuel injection across a wide range of engine operating regimes (e.g., low/high load at high speed, low/high load at low speed, and transient load–speed conditions). Therefore, this study aims to experimentally investigate the coupled influence of injection pressure, dwell time, and split ratio on the injection rate characteristics of a six-hole solenoid common-rail diesel injector. The main motivation of this study is to provide accurate experimental data for determining injection timing and fuel quantity, thereby enabling the proposal of optimized injection strategy adjustments under different engine operating conditions.

2.0 METHODOLOGY

2.1 Zeuch method principle

This study applied the Zeuch method [18, 19] to determine key fuel injection rate characteristics such as injection rate shapes, initiation time of injection periods, actual injection duration, and total injected mass. Figure 1 depicts the determination of the fuel injection rate using Zeuch's method, in which fuel is precisely introduced into a chamber under fixed volume at a given condition. In detail, the same type of test fuel was compressed to a predetermined pressure within this chamber to simulate the pressure condition of the diesel engine, like the compression stroke. In Zeuch's approach, the act of injecting fuel causes a measurable increase in chamber pressure, which correlates proportionally with the quantity of injected fuel. The increase in pressure ΔP (N/m^2) is determined by the following equation [26, 27]:

$$\Delta P = K.\frac{\Delta V}{V} \quad (1)$$

Where K (MPa) corresponds to the bulk modulus, which characterizes the fluid's resistance to compression, ΔV (m^3) is the volume of injected fuel, and V (m^3) is the chamber volume.

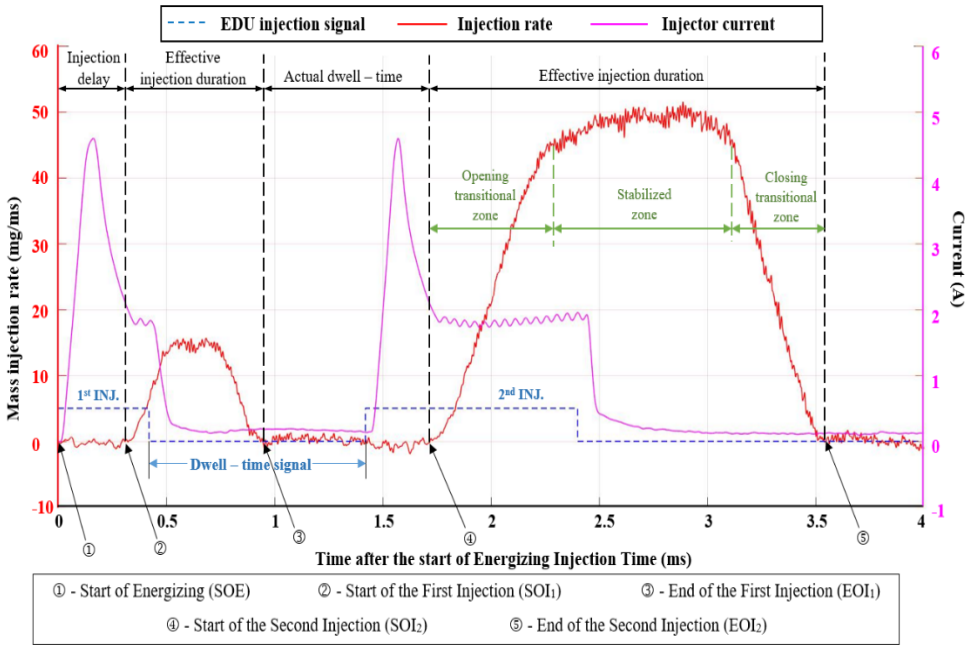

Figure 2 Illustration of a representative fuel injection rate profile under two-split injection strategies of 30%/70% (P_{inj} = 1600 bar, P_0 = 50 bar, DT=1.0 ms, and split inj.$_1$ =0.42 ms; split inj.$_2$ = 0.98 ms)

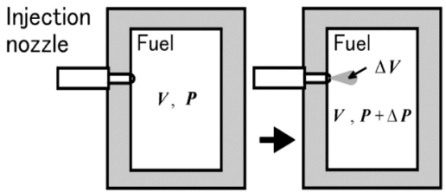

Figure 1 Injection rate measurement of Zuech [18]

The injection rate ($\dot{m}_f$) will subsequently be calculated using equation (2), derived from the measured pressure response under fixed-volume chamber conditions (1):

$$\dot{m}_f = \frac{d_m}{d_t} = p_f \frac{V}{K}\frac{\Delta P}{\Delta t} \quad (2)$$

where ρ_f (kg/m^3) represents the density of the test fuel.

The experimental injection rate profile for the two-split injection strategy, as analyzed from equation (2), is shown in Figure 2. This illustration reveals four distinct phases, namely the injection delay phase, the first split injection phase (1st effective injection duration), the actual dwell-time phase, and the second split injection phase (2nd effective injection duration) [28, 29]. The hydraulic injection delay is counted from the start of energizing (SOE, point 1) until the moment when fuel begins to emerge from the nozzle (SOI_1, point 2). The first injection timing is determined by the point on the injection rate curve where the transition occurs from a negative value (before injection) to a positive value (when injection begins) [11, 29, 30]. By contrast, the end of injection (EOI) is detected from a positive value to a negative value on the injection rate curve, corresponding to needle closure. The actual injection duration is computed as the time elapsed from the onset (SOI) until the termination of the injection event (EOI). The dwell-time signal refers to the electrical signal input to the control unit, while the actual dwell-time is the time interval between two effective successive injections, determined from EOI_1 (point 3) to SOI_2 (point 4). The maximum injection rate is determined by averaging the values in the vicinity of the injection rate peak. Finally, the amount of injection quantity is calculated by integrating the area under the injection rate characteristic curve from SOI to EOI for each shot injection.

2.2 Experimental Setup

Figure 3 and Figure 4 illustrate the actual test rig and the detailed schematic layout of the experimental apparatus. Specifications of the main component, which is the Zeuch testing chamber, occupy a volume of 43 cm^3 and will be pre-compressed at a fixed diesel fuel pressure of 50 bar by a hydraulic hand pump, which was similar to that compression pressure during the diesel compression stroke. A Denso electrical solenoid type G2 injector with a 6-hole nozzle is mounted above the Zeuch chamber and connected to a high-pressure fuel supply system, powered by an HP3 pump. This high-pressure pump operates through a three-phase motor, with its function managed via an inverter. The high-pressure common-rail fuel system (400–1800 bar) was calibrated using an ultra-high-pressure gauge (Wise EN837-1, range up to 200 MPa). To monitor the pressure conditions within the Zeuch

chamber, a static pressure sensor (Daho EDS 305) is employed to capture the back pressure, while a piezoelectric transducer (AVL GU12P) detects dynamic pressure changes during fuel injection with 130 kHz of sampling rate. The transducer has a nominal sensitivity of 15.35 pC/bar and a manufacturer-specified accuracy of ±0.5% of full scale. The sensor was factory-calibrated before use, and no additional calibration was performed during this study. The output signal from the piezo sensor is subsequently amplified using a Kistler 5010B charge amplifier before being sent to the data acquisition system. The high-pressure common-rail fuel system (400–1800 bar) was calibrated using an ultra-high-pressure gauge (Wise EN837-1, range up to 200 Mpa. Throughout the experiment, a microcontroller synchronizes the injector energizing signal, rail pressure signal, and transducer pressure signal in real-time, and is indicated by the Matlab program. The obtained data are then eventually analyzed and calculated by applying the injection rate equation (2). The parameters from injection rate curve are the average value obtained from 15 repetitions, and the error bar represents for standard deviation (SD).

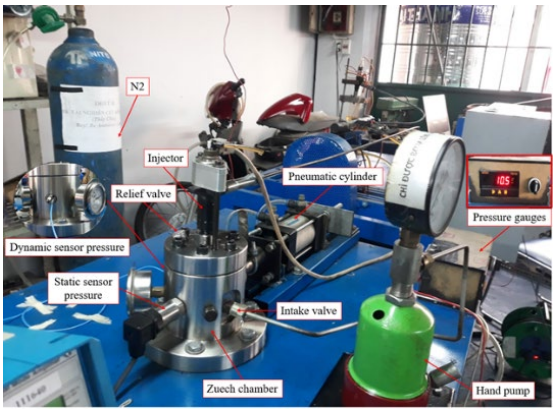

Figure 3 Actual test rig of the experimental setup

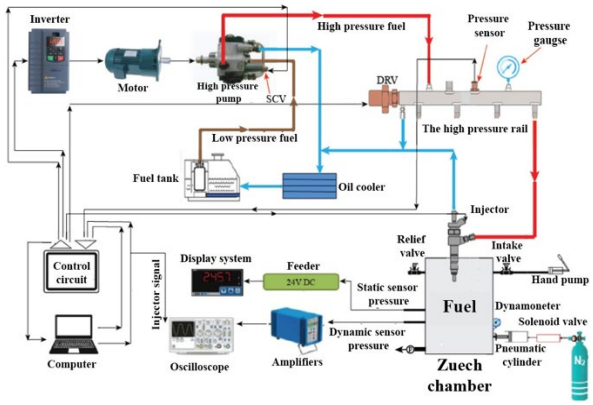

Figure 4 Schematic of experimental apparatus

2.3 Testing Procedure

The diesel fuel properties used in the study are displayed in Table 1.

Table 1 The Test Fuel Properties [31]

Parameter	Standard	Diesel
Density at 15°C (kg/m³)	ASTM D4052	840
Viscosity at 40°C (cSt)	ASTM D445	3.07
Cetane	ASTM D4737	46

The experimental conditions are summarized in Table 2, including variations in injection strategy, injection pressure, dwell time, and split ratio for the two-split mode. Experiments were performed using a G2 model 6-hole solenoid diesel injector, with fuel pressures ranging from 800 to 1600 bar and a fixed total energizing time of 1.4 ms. Both single-injection and split-injection strategies were employed, with dwell times varied from 0.2 ms to 1.8 ms for the two-split injections, and split ratios set at 30%/70%, 50%/50%, and 70%/30%.

Table 2 Testing Conditions

Parameters	Value	
Fuel	Diesel	
Injection pressure (Pinj)	800 bar; 1000 bar; 1200 bar; 1400 bar; 1600 bar	
	Single injection	**Two-split injection (split 1/ split 2)**
Injection strategies	0.42 ms; 0.7 ms; 0.98 ms; 1.4 ms	0.42 ms (30%)/ 0.98 ms (70%) 0.7 ms (50%)/ 0.7 ms (50%) 0.98 ms (70%)/ 0.42 ms (30%)
Dwell-time (DT)	-	0.2 ms; 0.6 ms; 1.0 ms; 1.4 ms; 1.8 ms
Back fuel pressure (Po)	50 bar	
Number of repetitions	15 times	
Injector type	Solenoid-actuated G2 model, 6 nozzle holes, diameter of 0.18 mm	

3.0 RESULTS AND DISCUSSION

3.1 Impact of Energizing Time on the Temporal Characteristics of Injection Rate under Single Injection Strategies

Figure 5 illustrates the fuel injection rate at different energizing times ranging from 0.42 ms to 1.4 ms under a single injection strategy, with an injection pressure of 1000 bar and a back pressure of 50 bar. As the energizing time increases, the shape of the injection rate curve changes significantly, consistent with the findings of C. Vo *et al*. [32], Wang *et al*. [33], and Payri *et al*. [34]. At a short energizing time of 0.42 ms, the injection rate rises slowly and reaches a lower peak because the needle valve does not fully lift due to insufficient electromagnetic force [35]. As the energizing time increases to 0.7 ms, 0.98 ms, and 1.4 ms, the peak shape evolves from triangular to semi-trapezoidal and eventually trapezoidal. This transition

reflects a more complete needle lift and an extended duration of the maximum injection rate at higher energizing times.

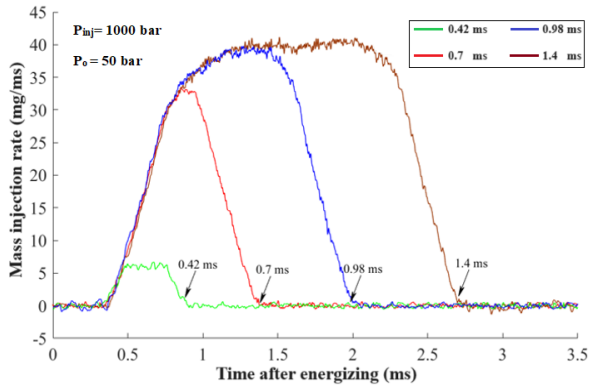

Figure 5 Effects of injector energizing time on nozzle rate of injection shape

The slower fuel pressure response at the needle tip during the closing signal introduces a delay in balancing the fuel compression force and the spring force inside the injector. Consequently, a triangular profile is observed at 0.7 ms and a trapezoidal profile becomes prominent at 0.98 ms and 1.4 ms, where the injector needle is fully lifted. The full opening of the needle valve results in a more stable and higher maximum injection rate. Specifically, the average injection rate in the vicinity of the fully open needle region at 0.7 ms, 0.98 ms, and 1.4 ms was 39.7 mg/ms, 41.6 mg/ms, and 40.1 mg/ms, respectively. This small variation may be attributed to cyclic pressure fluctuations in the common rail after each injection event [11, 36]. Additionally, the increasing slope of the injection rate curve during the opening phase remains similar for all energizing times, indicating consistent injection delay and needle lift stroke under the given injection pressure.

3.2 Impact of Energizing Time on Single Injection Duration

Figure 6 illustrates the comparison between the commanded energizing pulse and the actual injection time in the single injection strategy with an injection pressure of 1000 bar and a back pressure of 50 bar, energizing injection time ranging from 0.42 ms to 1.4 ms. The results show that the actual injection duration exceeds the injector energizing time and tends to increase with a higher energizing injection time. This is consistent with the trends observed by Tomasz Knefel [37] and Catania [35]. Specifically, regarding the energizing injection time of 0.42 ms, the actual injection duration is 0.58 ms, representing an increase of approximately 38.2%.

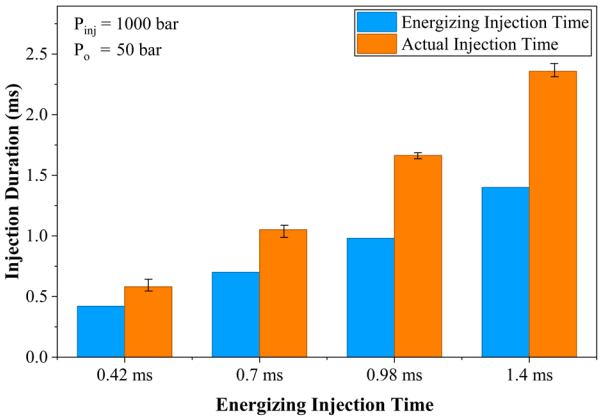

Figure 6 Effects of injector energizing time on the actual injection duration

The longer the injection's energizing time, the more distinctive the difference becomes. At the energizing injection time conditions of 0.7 ms, 0.98 ms, and 1.4 ms, the actual injection duration exceeds the energizing injection time by 50.1%, 69.8%, and 68.3%, respectively. This can be explained by the fact that a longer energizing injection time causes an increase in the time for electrical current to flow through the injector coil, generating a stronger electromagnetic force to lift the injector needle higher, along with the resistance of the compressed fuel beneath the injector needle and the longer closing travel as the needle is raised higher, which result in the extension of the actual injection duration.

3.3 Relationship between Energizing Time and Fuel Quantity

The mass of injected fuel at different energizing injection times, calculated by integrating the fuel injection rate curve, is presented in Figure 7. This figure illustrates the single injection strategy with energizing injection time varying from 0.42 ms to 1.4 ms, injection pressure of 1000 bar, and back pressure of 50 bar. The results reveal that the fuel injection amount increases with prolonged energizing injection time.

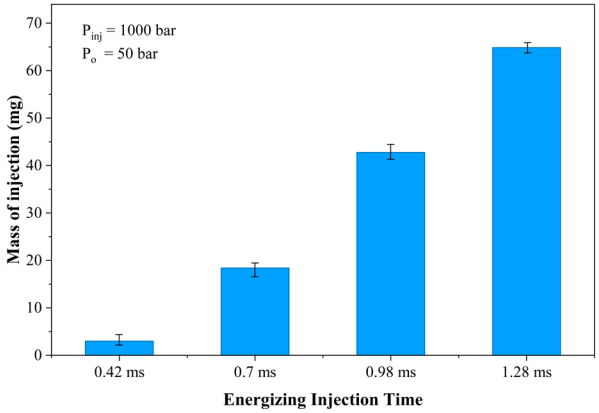

Figure 7 The relevance between injection energizing time and injection quantity

Specifically, the injected mass at 0.42 ms was 2.98 mg, and it increased to 18.4 mg and 42.75 mg at 0.7 ms and 0.98 ms, respectively. When the energizing time was further extended from 0.98 ms to 1.4 ms, the additional injected mass increased by only 22.09 mg, indicating a diminishing growth rate of fuel delivery. This result is attributed to the extension of the energizing injection time, resulting in the increased actual injection duration as mentioned in Section 3.2. Additionally, the initial stage of injection is characterized by a sharp increase in the injection rate, progressing toward its maximum level. However, when extending the energizing injection times from 0.98 ms to 1.4 ms, the phase of needle lift has already completed, followed by a fully opening needle phase, as observed in Figure 5.

3.4 Effects of Dwell-Time on Injection Rate under the 30%/70% Split Injection Strategies.

Figure 8 illustrates the diesel injection rate curve for the 30%/70% injection strategy, corresponding to the first and second split injections by 0.42 ms (30%)/ 0.98 ms (70%). The tests were conducted at a fuel injection pressure of 1000 bar and a back pressure of 50 bar, with the dwell time varied from 0.2 ms to 1.8 ms in increments of 0.4 ms. These obtained results are referenced to the single injection condition at the energizing injection time of 0.42 ms. The injection rate curve in the single injection strategy and the first split injection in the 30%/70% injection strategy at various dwell-times show insignificant differences in the initial process. On the other hand, the average quasi-steady state injection rate of the second split injection, with dwell-times ranging from 0.2 ms to 1.0 ms, exhibits a decreasing trend from 40.1 mg/ms to 38.5 mg/ms. However, as the dwell-times increase from 1.0 ms to 1.8 ms, the average quasi-steady state injection rate of the second split injection exhibits an upward tendency, rising from 38.5 mg/ms to 40.0 mg/ms.

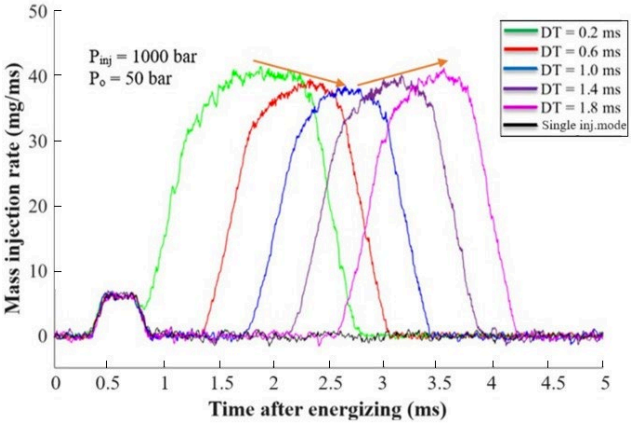

Figure 8 Effects of dwell-time on injection rate characteristics

As shown in Figure 9, the injected mass at a dwell-time (DT) of 0.2 ms is approximately 21.1% higher than that at a DT of 0.6 ms, where the two injections were clearly separated. These results are consistent with the findings reported by Vu H. Nguyen *et al*. [29]. It can be explained by the fact that a dwell-time of 0.2 ms is too short, leading to the partial overlap of the injection rate's slope of the first split injection with that of the second split injection. In other words, there is no clear separation between the two split injections in this strategy. Regarding dwell-times from 0.6 ms to 1.8 ms, due to the longer dwell-time, the injection process of the first split injection ends completely, and the injection rate curves become distinct from each other in the second split injection. A notable feature is detected in the injection rate curve during the mentioned dwell-times, from dwell-times of 0.6 ms to 1.0 ms, the quasi-steady injection rate of the second split injection decreases trend from 39.01 mg/ms to 38.5 mg/ms due to the influence of pressure oscillations, resulting in a reduction of the total injected fuel from 46.7 mg to 46.1 mg. The primary cause of this is attributed to the injection process occurring in the decreasing phase of the pressure wave in the first split injection, conversely, for the dwell-times from 1.0 ms to 1.8 ms, the extended dwell-time results in the injection process taking place in the increasing phase of the pressure wave in the second wave stage [36, 38]. This finding highlights how coherence dwell-time in two split injection strategies and the fuel pressure wave trend distinctly influence injection rate, changing the mass of injected fuel into the cylinder and impacting the fuel-air mixing ratio. As seen in Figure 8, within the range of dwell-times from 0.2 ms to 1.8 ms, the critical dwell-time in two-split injection strategies was identified. The critical dwell-time can be defined as the interval between split injections within the injection strategy, representing the point at which the injection rate profile exhibits a change in trend. The total injection quantity also varies in response to this critical dwell-time. If the second-split injection begins at the increasing side of the critical dwell-time, an increase in maximum injection rate is witnessed and vice versa, from 38.5 mg/ms to 40 mg/ms, as seen in Figure 9. At a dwell time of 1.0 ms, the quasi-steady-state injection rate was the lowest compared with the other dwell-times. Considering the implications for engine operation, especially under high-speed and high-load conditions where a large fuel quantity must be delivered within a short duration, it is recommended to avoid using a 1.0 ms dwell time. Instead, a dwell-time below this critical value should be considered to ensure sufficient fuel delivery and maintain optimal combustion performance.

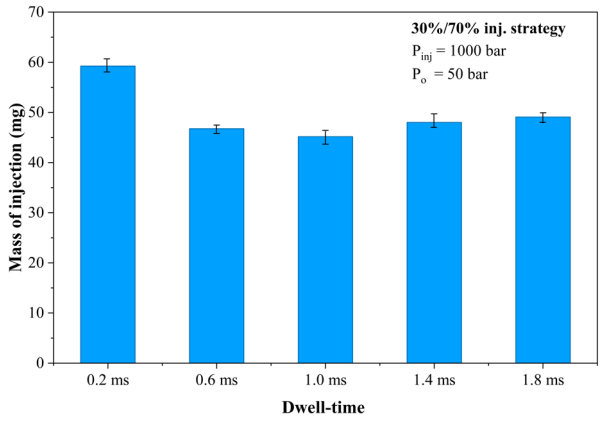

Figure 9 Effects of dwell-time on total quantity injection in the 30%/70% injection strategies

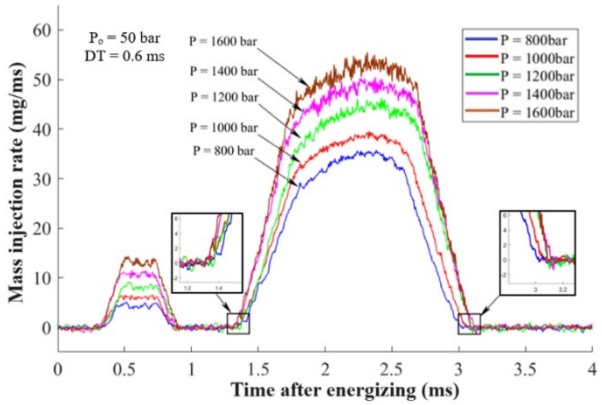

Figure 10 The influence of injection pressures on injection rate

3.5 Rate Profile Changes in Response to Pressure Variations under the 30%/70% Injection Strategy.

Figure 10 shows the influence of injection pressures on the diesel injection rate curve under conditions of the 30%/70% injection strategy, a constant dwell-time of 0.6 ms, a back pressure of 50 bar, and a progressive increase in injection pressure from 800 bar to 1600 bar. An upward trend in peak injection rate is observed in both split injections with increasing injection pressure. The slope of the injection rate curve in the second split injection highly increases during the needle lift transition phase. This may be caused by the high fuel pressure exerting a substantial thrust force on the injector needle as well as its longer moving distance, causing it to rapidly rise. Meanwhile, during the needle closing transition phase of the second split injection, the closing period is observed to increase progressively within the 800 to 1200 bar pressure range. On the other hand, as the injection pressure continues to increase from 1200 bar to 1400 bar and up to a very high 1600 bar, this phase remains almost unchanged. This is because the remaining high-pressure fuel in the lower distribution chamber below the needle resists the closing process, but as the injection pressure continues to rise and the compressibility of the fuel in the control chamber of the injector diminishes, expediting the needle's closing process and shortening the actual injection duration. Furthermore, in the quasi-steady injection rate stage of the second-split injection curves, it is noteworthy that the latter half exhibits a higher rate than the first half, reflecting the continued surge in injection rate. This can be explained by the turbulence level of the high-pressure fuel flow at the entrance hole inside the nozzle not only causing more vapor generation along the hole axis but also promoting the collapse of vapor bubbles before reaching the outlet. This reduction in flow detachment helps increase the effective flow area, resulting in a higher injection rate or in other words, lower primary breakup capacity. This predicts an increase in spray penetration [39].

3.6 Comparative Analysis of Injection Rate Profile across 50%/50% and 70%/30% Strategies: Pressure Effects and First-to-Second Injection Interactions

Figure 11 demonstrates the impact of fuel injection pressures on the injection rate curve in the 50%/50% injection strategy, with a constant dwell-time of 0.6 ms and a back pressure of 50 bar. The results indicate that applying the same injector energizing time for both injection events results in slightly greater variations in peak injection rate and actual duration during the second split injection phase compared to the first. This variation intensifies as fuel injection pressures increase, particularly noticeable at specific injection pressures, with a prominent example being 800 bar. In this scenario, during the steady phase, the second split injection achieves a rate of 28.1 mg/ms, signifying a 3.8% increase compared to the first split injection.

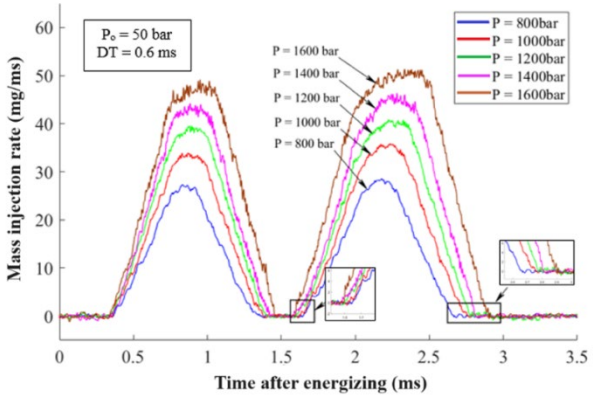

Figure 11 Comparative injection rate curves for the 50%/50% injection strategy across a range of injection pressures

Overall, this difference averages around 4.9% compared to the first split injection across all fuel injection pressures. Analysis of the injection rate curve indicates that the termination of the second split injection phase is significantly more prolonged compared to the first. This discrepancy may be

attributed to a slower needle closing process, contributing to an extended actual injection duration. Remarkably, with injection pressure varying between 800 and 1600 bar, the second split injection shows a 4.1% to 13.7% longer actual duration than the first. The rise in injection pressure leading to reduced effective dwell-times, resulting in fluctuations in both the maximum injection rate and the actual injection duration can be recognized as the primary cause. In addition, the ending duration of the second split injection increases steadily from the injection pressure of 800 bar to 1600 bar. In contrast, with the 30%/70% injection strategy, this interval only increases from 800 bar to 1200 bar, remaining nearly unchanged from 1200 bar to 1600 bar (as shown in Figure 10). This suggests that with a short injector energizing time (0.7 ms in the 50%/50% strategy), the fuel bulk modulus in the volume chamber had a negligible impact on the needle closing process.

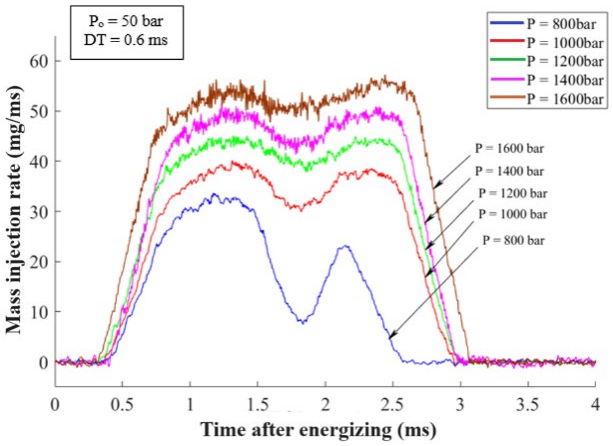

Figure 12 The impact of fuel injection pressures on the injection rate characteristics under the 70%/30% injection strategy

Figure 12 presents the injection rate profiles at various injection pressures under the 70%/30% split strategy, with a constant dwell-time of 0.6 ms and a back pressure of 50 bar. The results indicate that, among all injection strategies with the same dwell-time, only the 70%/30% injection strategy exhibits overlapping injection rate curves between the two injections when compared to the 30%/70% and 50%/50% strategies. As shown in Figure 12, there is no distinct separation between the injection intervals for the first and second split injections. To be specific, in the 30%/70% injection strategy, the actual dwell-time ranges from approximately 0.41 ms to 0.48 ms. In the 50%/50% injection strategy, it varies from 0.07 ms to 0.31 ms across all injection pressures. Regarding actual injection duration in this injection strategy, when injection pressure is changed from 800 bar to 1600 bar, the actual injection duration for two split injections increases from 20% to 70% compared to the total energizing injection time of 1.4 ms.

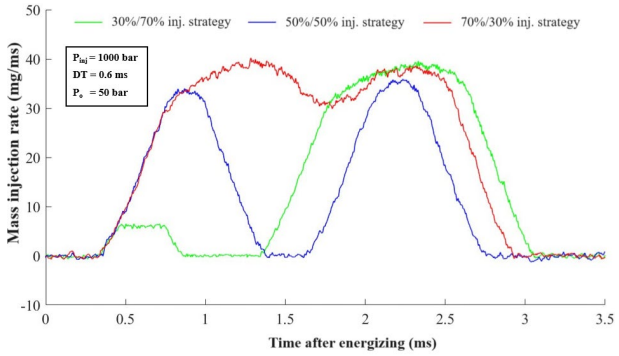

Figure 13 Effects of the different injection strategies on the injection rate under the injection pressure of 1000 bar and a dwell-time of 0.6 ms

In Figure 13, it is evident that changing the injection strategy does not influence the injection timing (i.e., the injection delay remains the same), but it significantly affects the total injection quantity. The overlapping profiles of the injection rate curves suggest that during the heat absorption phase for vaporization, the first and second split injections can influence the ignition delay. This, in turn, changes the combustion timing and impacts various stages of the combustion process as well as the heat release rate. In other words, the evolution of the injection rate profile affects engine noise and the smoothness of transitions during sudden changes in load or speed, while the total injection quantity influences engine power and emissions [40, 41].

3.7 Effects of Injection Pressures on Injection Quantity under Various Injection Strategies

Figure 14 presents a comparison of fuel quantities injected at pressures between 800 and 1600 bar, keeping the back pressure fixed at 50 bar and the dwell-time at 0.6 ms, under the same total injection period. Both single injection and split injection strategies with ratios of 30%/70%, 50%/50%, and 70%/30% are evaluated. The results clearly show that, despite consistent total injection energizing times across all strategies, there is a significant disparity in mass. Among injection strategies, at 800 bar of injection pressure as a reference point, the single-shot strategy achieves the highest injection mass by 61.9 mg, while the 50%/50% strategy records the lowest at 29.6 mg, with the 70%/30% and 30%/70% strategies displaying similar injection quantities. This variation results from the longer difference (Δt) between actual injection length and energizing injection time in the single-injection strategy compared to the split injection strategy. Moreover, boosting the pressure from 800 to 1600 bar proportionally improves the effectiveness of the single-shot injection strategy.

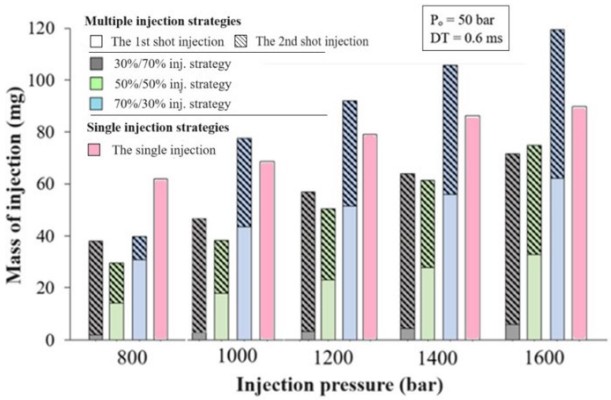

Figure 14 The comparison of injection quantity under various injection strategies and injection pressures

Notably, significantly higher injection quantities are observed in the 70%/30% injection strategy compared to the single injection strategy, particularly noticeable in the second split injection. This can be explained by the prolonged duration of the first split injection, which increases turbulence levels at the entrance hole alongside the pressure wave generation during the first split injection, increasing flow velocity. Consequently, this leads to higher injection rates, as observed in Figure 13. Under conditions of the same injection pressure (800 bar to 1200 bar) for the 50%/50% injection strategy, the results reveal that the injection quantity is lower than that of the 30%/70% injection strategy. However, as the injection pressure rises from 1400 bar to 1600 bar, there is a clear trend towards higher fuel injection mass. Also, within this strategy, the 2nd shot injection mass consistently surpasses the first, especially evident at 1600 bar, where it exceeds the first by 29.08%. Based on the above analysis, the 30%/70% or 50%/50% split injection strategies, characterized by a smaller initial fuel quantity compared with the 70%/30% strategy, resulting in shorter ignition delay and a reduced premixed-combustion phase, are considered optimal for engine operation under low- to medium-load conditions. These strategies may help reduce combustion noise, decrease NO_x emissions, and improve combustion stability [23]. In contrast, the single injection strategy is more suitable for high-load conditions, where a large fuel quantity must be delivered within a short duration, although it generally leads to higher emissions and increased combustion noise. Under high-load and low-speed conditions, the 70%/30% split injection strategy may be considered, as it provides increased injected fuel mass and a longer actual injection duration compared with a single injection. Moreover, the split injection characteristic in this strategy helps control the heat release rate, preventing excessively rapid combustion, thereby reducing peak cylinder pressure and NO_x emissions due to a more uniform combustion temperature distribution.

4.0 CONCLUSION

The conclusions of this study are based on an experimental investigation of the injection dynamics of a six-hole solenoid diesel injector operated at various dwell times and injection pressures under both single and split injection strategies in a Zeuch chamber. In the single injection strategy, a slower fuel pressure response at the needle tip delays the equilibrium between fuel compression and injector spring forces, producing distinct injection rate profiles. Trapezoidal and triangular shapes are observed at ETs of 0.42 ms and 0.7 ms, respectively, while longer energizing times of 0.98 ms and 1.4 ms allow full needle lift, resulting in a clearly trapezoidal profile. For the split injection strategy, during the second injection event, the quasi-steady stage injection rate decreases from 40.1 mg/ms to a minimum of 38.5 mg/ms at a DT of 1.0 ms, before increasing again to 40 mg/ms. This indicates that a 1.0 ms dwell time may be unsuitable under high-speed and high-load conditions, where sufficient fuel delivery within a short duration is critical to maintaining optimal combustion. Very short dwell times, such as 0.2 ms, lead to the merging of the two injection events, increasing the total injected fuel by approximately 21.1% compared with a 0.6 ms dwell time, where the two injection profiles are clearly separated. This highlights the importance of dwell-time selection in controlling fuel distribution, combustion behavior, and engine operation during transient load and speed conditions to ensure stable combustion control. The 30%/70% or 50%/50% split injection strategies are considered optimal for low- to medium-load conditions, as they reduce combustion noise, lower NOx emissions, and improve overall combustion stability. In contrast, the single injection strategy is more suitable for high-load operation, where rapid delivery of a large fuel quantity is required. The 70%/30% split injection strategy, on the other hand, enhances heat absorption, induces a cooling effect, and moderates the spray temperature, helping to control the peak cylinder pressure and the heat release rate during combustion, making it suitable for high-load and low-speed conditions.

Acknowledgement

We acknowledge the support of time and facilities from Industrial University of Ho Chi Minh City (IUH) for this study.

Conflicts of Interest

The authors declare that there is no conflict of interest regarding the publication of this paper.

References

[1] Sindhu, R., G. Amba, P. R. Madhu. 2018. Effective Reduction of NOx Emissions from Diesel Engine Using Split Injections. *Alexandria Engineering Journal.* 57: 1379–1392. https://doi.org/10.1016/j.aej.2017.06.009.

[2] Gurumoorthy, S. H. 2014. NOx from Diesel Engine Emission and Control Strategies: A Review. *International Journal of Mechanical Engineering and Robotics Research.* 3: 471–479.

[3] Kun, L. T., W. Yang, F. Zhang, W. Yang, and M. Balaji. 2017. A Numerical Study on the Effects of Boot Injection Rate Shapes on the Combustion and Emissions of a Kerosene–Diesel Fueled Direct Injection Compression Ignition Engine. *Fuel.* 203: 430–444. https://doi.org/10.1016/j.fuel.2017.04.142.

[4] Ferrari, A., A. Mittica, F. Paolicelli, and P. Pizzo. 2016. Hydraulic Characterization of Solenoid-Actuated Injectors for Diesel Engine Common Rail Systems. *Energy Procedia.* 101: 878–885. https://doi.org/10.1016/j.egypro.2016.11.111.

[5] Keiki, T., S. Kato, and S. Nakakita. 2005. Effect of Fuel Injection Rate Control on Reduction of Emissions and Fuel Consumption in a Heavy-Duty DI Diesel Engine. *SAE Technical Paper.* 2005-01-0907. https://doi.org/10.4271/2005-01-0907.

[6] Chad, K., G. Martin, T. Bodisco, W. Milton, K. Stetter, and C. G. Jordan. 2015. The Influence of Diesel End-of-Injection Rate Shape on Combustion Recession. *SAE International Journal of Engines.* 8: 647–659. https://doi.org/10.4271/2015-01-0795.

[7] Han, S., J. Song, *et al*. 2015. Coordinated Control Strategy for the Common-Rail Pressure Using a Metering Unit and a Pressure Control Valve in Diesel Engines. *Proceedings of the Institution of Mechanical Engineers, Part D: Journal of Automobile Engineering.* 229(7): 898–911. https://doi.org/10.1177/0954407014549060.

[8] Benajes, J., S. Molina, K. De Rudder, and T. Rente. 2006. Influence of Injection Rate Shaping on Combustion and Emissions for a Medium-Duty Diesel Engine. *Journal of Mechanical Science and Technology*. 20: 1436–1448. https://doi.org/10.1007/BF02915967.

[9] Xu, L., X. Bai, M. Jia, Y. Qian, X. Qiu, and X. Li. 2018. Experimental and Modeling Study of Liquid Fuel Injection and Combustion in Diesel Engines with a Common Rail Injection System. *Applied Energy*. 230: 287–304. https://doi.org/10.1016/j.apenergy.2018.08.104.

[10] Prashanth, K., and S.-C. Kong. 2009. Diesel Emission Characteristics Using High Injection Pressure with Converging Nozzles in a Medium-Duty Engine. *SAE International Journal of Fuels and Lubricants.* 1: 578–592. https://doi.org/10.4271/2008-01-1085.

[11] Dong, H., Y. Du, C. Wang, L. He, and Z. Hu. 2014. Experimental Study on Injection Characteristics of Fatty Acid Esters on a Diesel Engine Common Rail System. *Fuel.* 123: 19–25. https://doi.org/10.1016/j.fuel.2014.01.048.

[12] Julien, M., A. Kastengren, and R. Payri. 2012. Understanding the Acoustic Oscillations Observed in the Injection Rate of a Common-Rail Direct Injection Diesel Injector. *Journal of Engineering for Gas Turbines and Power.* 134(12): 122801. https://doi.org/10.1115/1.4007276.

[13] Payri, A., G. Bracho, F. Margot, A. Correas, L. Postrioti, and F. C. Payri. 2017. Experimental and Numerical Assessment of Multi-Event Injection Strategies in a Solenoid Common-Rail Injector. *SAE International Journal of Engines.* 10: 2129–2140. https://doi.org/10.4271/2017-24-0012.

[14] Corcione, A. E., A. Ferrari, and E. Spessa. 2006. Numerical–Experimental Study and Solutions to Reduce the Dwell Time Threshold for Fusion-Free Consecutive Injections in a Multijet Solenoid-Type Common-Rail System. In *Proceedings of the Internal Combustion Engine Division Spring Technical Conference*. 317–332. https://doi.org/10.1115/ICES2006-1369.

[15] Postrioti, L., A. Cavicchi, and D. Pennacchi. 2016. An Experimental and Numerical Analysis of Pressure Pulsation Effects of a Gasoline Direct Injection System. *Fuel.* 173: 8–28. https://doi.org/10.1016/j.fuel.2016.01.012.

[16] Ramazan, S., Murat U. Y., and Mehmet Z. G. 2020. Effects of Injection Strategy and Combustion Chamber Modification on a Single-Cylinder Diesel Engine. *Fuel.* 266: 117122. https://doi.org/10.1016/j.fuel.2020.117122.

[17] Phuong, X. P., Kien T. N., Thin V. P., and Vu H. N. 2020. Biodiesels Manufactured from Different Feedstock: From Fuel Properties to Fuel Atomization and Evaporation. *ACS Omega.* 5: 20842–20853. https://doi.org/10.1021/acsomega.0c02083.

[18] Ishikawa, S., Ohmori Y., Fukushima S., Suzuki T., Takamura A., and Kamimoto T. 2000. Measurement of Rate of Multiple-Injection in CDI Diesel Engines. *SAE Technical Paper.* 2000-01-1257. https://doi.org/10.4271/2000-01-1257.

[19] Lucio, P., Giacomo B., Francesco C. P., and Claudio C. 2014. Zeuch Method-Based Injection Rate Analysis of a Common-Rail System Operated with Advanced Injection Strategies. *Fuel.* 128: 188–198. https://doi.org/10.1016/j.fuel.2014.03.006.

[20] Simón, M., Oscar A. G., Miguel G. Y., Ricardo M. C., and Fausto A. S. C. 2021. Hydraulic Interactions between Injection Events Using Multiple Injection Strategies and a Solenoid Diesel Injector. *Energies.* 14(11): 3087. https://doi.org/10.3390/en14113087.

[21] Raul, P., Pedro M. A., Tomas M., and Alberto V. 2020. Influence of Aging of a Diesel Injector on Multiple Injection Strategies. *Applied Thermal Engineering.* 181: 115891. https://doi.org/10.1016/j.applthermaleng.2020.115891.

[22] Su, H. P., Hyung J. K., and Chang S. L. 2016. "Effect of Multiple Injection Strategies on Combustion and Emission Characteristics in a Diesel Engine. *Energy & Fuels.* 30(2): 810–818. https://doi.org/10.1021/acs.energyfuels.5b02121.

[23] Sindhu, R., Amba P. R. G., and Madhu M. K. 2018. Effective Reduction of NOx Emissions from Diesel Engine Using Split Injections. *Alexandria Engineering Journal.* 57(3): 1379–1392. https://doi.org/10.1016/j.aej.2017.06.009.

[24] Nehmer, D. A., and Reitz, R. D. 1994. Measurement of the Effect of Injection Rate and Split Injections on Diesel Engine Soot and NOx Emissions. *SAE Transactions.* 103: 1030–1041. https://doi.org/10.4271/940668.

[25] Beatrice, C., Belardini P., *et al*. 2002. Diesel Combustion Control in Common Rail Engines by New Injection Strategies. *International Journal of Engine Research.* 3(1): 23–36. https://doi.org/10.1243/1468087021545513.

[26] Andrea, P., Federico M., Lucio P., Giulia B., Andrea C., and Francesco C. P. 2016. Numerical and Experimental Assessment of a Solenoid Common-Rail Injector Operation with Advanced Injection Strategies. *SAE International Journal of Engines.* 9: 565–575. https://doi.org/10.4271/2016-01-0563.

[27] Changhee, L. 2016. An Experimental Study on Advanced Injection Rate Measurement of a Marine Engine Using the Zeuch Method. *Journal of Thermal Science and Technology*. https://doi.org/10.1299/jtst.2016jtst0026.

[28] Junkyu, P., Ji H. J., and Sungwook P. 2015. Effect of Fuel Temperature on Heavy Fuel Oil Spray Characteristics in a Common-Rail Fuel Injection System for Marine Engines. *Ocean Engineering.* 104: 580–589.

[29] Vu, H. N., Andrea C., Dat X. N., Kien T. N., Phuong X. P., and Lucio P. 2022. Hydraulic Characterization of a Second-Generation Common Rail Injector Operating under Solo and Split Injection Strategies. *Flow Measurement and Instrumentation.* 85: 102170. https://doi.org/10.1016/j.flowmeasinst.2022.102170.

[30] Munsin, R., Laoonual Y., Jugjai S., Matsuki M., and Kosaka H. 2015. Effect of Glycerol Ethoxylate as an Ignition Improver on Injection and Combustion Characteristics of Hydrous Ethanol under CI Engine Condition. *Energy Conversion and Management.* 98: 282–289. https://doi.org/10.1016/j.enconman.2015.03.116.

[31] PETROLIMEX. 2011. DO Oil. Accessed September 5, 2023. https://kv5.petrolimex.com.vn/nd/linhvuc-kd/nhien_lieu_diezen.html.

[32] Vo, T. C., Tran D. L., Huynh B. V., *et al*. 2023. A Study on the Injection Rate Characteristics of the Solenoid Common-Rail Injector Using a High-Pressure Fuel System. *Jurnal Teknologi*. 85(3): 25–33. https://doi.org/10.11113/jurnalteknologi.v85.19106.

[33] Ziman, W., and Miroslaw L. W. 2015. Fuel Injection and Combustion Study by the Combination of Mass Flow Rate and Heat Release Rate with Single and Multiple Injection Strategies. *Fuel Processing Technology*. 132: 118–132. https://doi.org/10.1016/j.fuproc.2014.11.024.

[34] Raul, P., Antonio G., Vicent D., Russell D., and Alejandro H. P. 2012. An Experimental Study of Gasoline Effects on Injection Rate, Momentum Flux and Spray Characteristics Using a Common Rail Diesel Injection System. *Fuel*. 97: 390–399. https://doi.org/10.1016/j.fuel.2011.11.065.

[35] Andrea, E. C., Alessandro F., and Ezio S. 2006. Numerical-Experimental Study and Solutions to Reduce the Dwell Time Threshold for Fusion-Free Consecutive Injections in a Multijet Solenoid-Type CR System. *Journal of Engineering for Gas Turbines and Power*. 131(2): 317–332. https://doi.org/10.1115/ICES2006-1369.

[36] Andrea, E. C., Alessandro F., Michele M., and Ezio S. 2008. Experimental Investigation of Dynamic Effects on Multiple-Injection Common Rail System Performance. *Journal of Engineering for Gas Turbines and Power*. 130: 032806. https://doi.org/10.1115/1.2835353.

[37] Knefel, T. 2011. The Evaluation of the Characteristic Injection Times of a Multiple Fuel Dose. *Journal of KONES*. 18: 205–213.

[38] Andrea, C., and Lucio P. 2019. Hydraulic Analysis of a GDI Injector Operation with Close Multi-Injection. *Fuel*. 235: 1114–1122. https://doi.org/10.1016/j.fuel.2018.08.089.

[39] Federico, B., Stefania F., and Piero P. 2014. Influence of the Diesel Injector Hole Geometry on the Flow Conditions Emerging from the Nozzle. *Energy Procedia*. 45: 749–758. https://doi.org/10.1016/j.egypro.2014.01.080.

[40] Dong, H., Yaozong D., Chunhai W., He L., Zhen H., and Margaret S. W. 2016. Experimental Study of the Two-Stage Injection Process of Fatty Acid Esters on a Common Rail Injection System. *Fuel*. 163: 214–222. https://doi.org/10.1016/j.fuel.2015.09.066.

[41] Carlos, J. M., Ola St., and Per T. 2017. Investigation of Small Pilot Combustion in a Heavy-Duty Diesel Engine. *SAE International Journal of Engines*. 10: 1193–1203. https://doi.org/10.4271/2017-01-0718.